

Quality Assessment of a 1985–2007 Mediterranean Sea Reanalysis

MARIO ADANI

Gruppo Nazionale di Oceanografia Operativa, INGV, Sezione di Bologna, Bologna, Italy

SRDJAN DOBRICIC

Centro EuroMediterraneo per i Cambiamenti Climatici, Bologna, Italy

NADIA PINARDI

Department of Environmental Sciences, University of Bologna, Ravenna, Italy

(Manuscript received 12 May 2010, in final form 23 September 2010)

ABSTRACT

A simulation and two reanalyses from 1985 to 2007 have been produced for the Mediterranean Sea using different assimilation schemes: a reduced-order optimal interpolation [System for Ocean Forecast and Analysis (SOFA)] and a three-dimensional variational scheme (OceanVar). The observational dataset consists of vertical temperature and salinity in situ profiles and along-track satellite sea level anomalies; daily mean fields of satellite sea surface temperature are used for correcting the air–sea fluxes. This paper assesses the quality of the reanalyses with respect to observations and the simulation.

Both the SOFA and OceanVar schemes give very similar root-mean-square errors and biases for temperature and salinity fields compared with the assimilated observations. The largest errors are at the thermocline level and in regions of large eddy field variability. However, OceanVar gives 20% better results for sea level anomaly root-mean-square error.

1. Introduction

Global ocean reanalysis is a consolidated technique in oceanography that allows the production of a consistent, three-dimensional estimate of ocean circulation from observations and model simulations. Here we follow the meteorological definition of reanalysis (Glickman 2000; see online at <http://amsglossary.allenpress.com/glossary>), which states that a reanalysis is like an analysis done with a consistent model and data assimilation scheme for the period of interest, yielding to a temporally homogeneous gridded dataset. Several techniques have been utilized in the past to produce large-scale reanalyses: the partitioned Kalman filter (Fukumori 2002), variational methods (Masina et al. 2004), and optimal interpolation (OI; Carton et al. 2000). Ocean observations are usually taken either from satellite altimetry (Fu et al. 1994) or in

situ data, and only a few reanalyses use both datasets (Stammer et al. 2002). Regional reanalyses are challenging because observational datasets may be scarcer at regional levels, and higher-resolution models are required to represent the dynamics correctly (Douglass et al. 2009).

The advent of operational oceanography (Pinardi and Woods 2002) and the setup of real-time monitoring systems now allows high-resolution regional ocean reanalyses with a relevant number of observations and calibrated models to be carried out for the first time. In this paper we will describe the first ocean reanalysis for the Mediterranean Sea carried out for the time period of 1985–2007 using all of the available historical in situ and satellite data and the operational forecasting model calibrated and validated over the past 10 yr (Pinardi et al. 2003; Tonani et al. 2008b).

The Mediterranean Sea is a semienclosed sea located between 5°E and 36°W and between 32° and 46°N with average depth of 1500 m. It communicates with the Atlantic through the Strait of Gibraltar and with the Marmara Sea through the Dardanelles. The Mediterranean

Corresponding author address: Mario Adani, via Aldo Moro 44, Istituto Nazionale di Geofisica e Vulcanologia, 41100 Bologna, Italy.
E-mail: adani@bo.ingv.it

circulation is forced by all the traditional forcings of the circulation, from the wind to the air–sea heat and water fluxes. The wind stress is the main factor responsible for the permanent gyres of the basin (Pinardi and Masetti 2000). The heat and water fluxes control the thermohaline circulation, which is forced by deep-water formation processes in the northern part of the basin. The Strait of Gibraltar net heat and water volume inflow maintains the long-term heat and water balance of the basin. The Mediterranean Sea has a negative water budget in which the evaporation exceeds the precipitation and the river runoff, so that the equilibrium is maintained by gaining water from the Atlantic. The basin also shows a net loss of heat [$O(10 \text{ W m}^{-2})$] that is balanced by the net positive gain of heat from the Strait of Gibraltar. These two features produce an antiestuarine circulation with an interface at Gibraltar of about 150 m.

Recent studies have demonstrated that the Mediterranean circulation is due to a particular equilibrium between mesoscales and seasonal and interannual variability (Robinson et al. 2001; Demirov and Pinardi 2007); the strong interaction between the different scales makes it difficult to study the Mediterranean circulation. Moreover, the two subbasins show a different behavior: in the western basin the seasonal variability dominates, while in the eastern basin both the seasonal and interannual signals are present (Korres et al. 2000). The construction of a reanalysis will allow for the renewed study of the seasonal and interannual variability of the Mediterranean Sea with a homogeneous time series of gridded data at unprecedented resolution.

A fundamental part of a reanalysis system is the data assimilation scheme, which minimizes the cost function constructed with the misfits between the observations and the numerical simulation or hindcast with the constraint of the model equations and their parameters. Although data assimilation theory is well known, its practical implementation is challenging for most state-of-the-art ocean general circulation models (OGCMs) because computational requirements are high. To overcome this problem different approximations have been proposed in the past, producing approximated assimilation schemes. In this work we will compare an optimal interpolation scheme, or rather, a reduced-order optimal interpolation scheme called the System for Ocean Forecast and Analysis (SOFA; De Mey and Benkiran 2002), with a three-dimensional variational scheme called OceanVar, developed by Dobricic and Pinardi (2008). Furthermore, the different estimates will be compared with observations and the simulation in order to assess the overall quality of the reanalysis and the sensitivity of the ocean-state estimates to the assimilation scheme.

TABLE 1. List of experiments and names.

Expt name	Description
SIM	Forced simulation
OV-RE	Reanalysis using OceanVar scheme of Dobricic and Pinardi (2008)
SO-RE	Re-analysis using SOFA (De Mey and Benkiran 2002)

The paper is organized as follows: a comprehensive description of the data assimilation schemes, model, and data used to produce the reanalysis is given in section 2; results will be shown in section 3; and a discussion and conclusions are presented in section 4.

2. Experimental setup

Three numerical experiments have been performed and intercompared; they are listed in Table 1. The simulation (SIM) and the reanalysis done with OceanVar (OV-RE) have been initialized from 1 January 1985 from the temperature and salinity monthly mean MedAtlas climatology (Maillard et al. 2005) and have been integrated continuously for 23 yr. The reanalysis done with SOFA (SO-RE) has been subdivided into the following three parts: one from 1985 to 1990, initialized as SIM and OV-RE; the second from 1993 to 1995; and the last from 2000 to 2007. The last two have been initialized from OV-RE restarts. The periods of SO-RE were chosen on the basis of observation availability in order to perform the intercomparison exercise. In the first period (1985–90), there were many in situ measurements but no satellite data; the second period (1993–95) corresponds to the beginning of the satellite altimetry; and the third period was chosen because there was a good combination of in situ and satellite measurements (2000–07).

a. Model system description

The OGCM used in this work is based on Océan Parallélisé (OPA) 8.1 code (Madec et al. 1998), which has been implemented in the Mediterranean Sea by Tonani et al. (2008a). The model has 1/16th horizontal resolution and 71 unevenly spaced vertical levels. The model domain is shown in Fig. 1; the Atlantic box is closed and no slip lateral boundary conditions have been used. The model equations and vertical boundary conditions are briefly presented in appendix A. The difference between Tonani et al.'s (2008a) implementation and the one used in this paper concerns the water flux (WF) parameterization, which is used as a surface boundary condition for the salinity, as shown in Eq. (A16). In the present formulation of the water flux [Eq. (A17)],

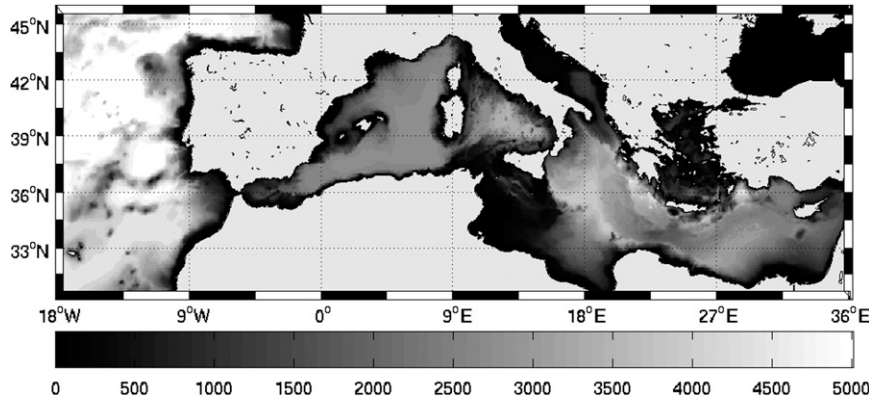


FIG. 1. Bathymetry (m) of the model. The number corresponds to the location of the freshwater input expressed in Eq. (1) as \mathbf{R} . In particular, Eq. (A17) corresponds to Bojana, Eq. (2) to Seman, Eq. (3) to Vjiose, Eq. (4) to Dardanelles, Eq. (5) to Nile, Eq. (6) to Ebro, Eq. (7) to the Po, and Eq. (8) to Rhone.

precipitation (P) is taken from the climatological monthly mean fields of the National Centers for Environmental Prediction–National Center for Atmospheric Research (NCEP–NCAR) reanalysis (Kistler et al. 2001), and it is interpolated from the original resolution grid of the reanalysis (T-62, about 320 km) to the model grid points. Precipitation has not been interpolated in time, but it is used as step function in which, for the first day of each month, the values of the precipitation change at each grid point. Evaporation E is computed with interactive bulk formulas (Tonani et al. 2008a) at each time step and in each model grid point. River discharge (R ; $\text{m}^3 \text{s}^{-1}$) is multiplied by a Gaussian function [Eq. (A18)] at the river mouth in order to disperse the amount of freshwater that is not in one single grid point near the coast, but is instead in several grid points in the offshore direction; the purpose of this calculation is to parameterize the river plume inside the sea. The zero-crossing parameter (L) has been chosen as being equal to 80 km at the Dardanelles, which is considered herein as a river mouth, and 60 km for the other rivers. The e -folding parameter (B) for the Dardanelles is 40 and 10 km for the other rivers. Both the L and B parameters have been experimentally decided, according to the general philosophy that the more abundant the river discharge, the bigger the area in which the runoff is spread. This formulation may help to avoid numerical instabilities because of the large salinity gradients.

The runoff data have not been time interpolated, but they have been used as the already described precipitation. The implemented rivers and runoff data are the same as those used in Oddo et al. (2009). The location and the name of the rivers are shown in Fig. 1.

Both SO-RE and OV-RE correct the model SST by means of a heat flux correction term [Eq. (A14)], which

is proportional to the difference between the model and the observed SST (Pinardi et al. 2003). The relaxation coefficient is equal to $-60 \text{ W m}^{-2} \text{ K}^{-1}$, corresponding to about 2.5 days.

In all three experiments the following atmospheric forcing has been used: from 1985 to 1992 the 15-yr European Centre for Medium-Range Weather Forecasts (ECMWF) Re-Analysis (ERA-15; Gibson et al. 1997), and from 1993 to 2007 the operational ECMWF analyses. This sequence of the forcing fields was chosen because ECMWF operational analyses have higher spatial resolution, which is believed to be important for reproducing the correct air–sea interactions (Bozec et al. 2006). The model utilizes the surface atmospheric fields and computes heat, momentum, and water fluxes using the model SST, as explained in Tonani et al. (2008a). In the bulk formulas, the cloud cover for the period of 1985–92 has been taken from the NCEP–NCAR reanalysis because this field was thought to be unreliable from ERA-15, while for the subsequent period ECMWF operational cloud cover analysis values are used. ERA-15 covers the period from 1979 to 1993 and the operational analyses were at the same resolution for this period because in both cases the model employed was T105. After 1991, the ECMWF operational products became higher resolution (in 1991 the model increased to T213 resolution, in 1998 to T319 resolution, and in 2000 to T511 resolution), and they used an improved assimilation scheme [in 1996 ECMWF changed from OI to three-dimensional variational data assimilation (3DVAR), and in 1997 it changed again to four-dimensional variational data assimilation (4DVAR)]. Thus, our choice for ERA-15 was mandatory; moreover, Demirov and Pinardi (2002, 2007) showed that this combined forcing dataset could give reasonable simulation results. We could have

used the 40-yr ECMWF Re-Analysis (ERA-40), which uses the T213 model, but in any case we would have changed to ECMWF operational analyses in 1998, thus producing a discontinuity in the forcing. The decision to use climatological monthly mean precipitation from NCEP–NCAR reanalysis instead of ERA-15 has been driven by the fact that NCEP–NCAR reanalysis covers the entire period of the reanalysis presented in this work. Because precipitation is closely related to cloud cover field, the NCEP–NCAR reanalysis cloud cover also has been used.

The model output consists of daily mean fields of temperature, salinity, currents, sea surface height (SSH), wind stress, heat flux, water flux, and shortwave radiation.

b. Data assimilation schemes

The first assimilation scheme used is SOFA, which is implemented by De Mey and Benkiran (2002) and Demirov and Pinaridi (2002) and upgraded by Dobricic et al. (2005, 2007). In SOFA the analyses \mathbf{x} are obtained by adding increments to the background state \mathbf{x}_b by

$$\mathbf{x} = \mathbf{x}_b + \mathbf{B}\mathbf{H}^T(\mathbf{H}\mathbf{B}\mathbf{H}^T + \mathbf{R})^{-1}[\mathbf{y} - \mathcal{H}(\mathbf{x})], \quad (1)$$

where \mathbf{B} is the background error covariance matrix, \mathbf{R} is the observational error covariance matrix, \mathbf{y} is the vector of observations, \mathcal{H} is the observational operator, and \mathbf{H} is its linear approximation.

The background error covariance matrix is written as

$$\mathbf{B} = \mathbf{\Sigma}^T \mathbf{B}_r \mathbf{\Sigma}, \quad (2)$$

where $\mathbf{\Sigma}$ contains vertical multivariate EOFs calculated for the Mediterranean Sea by Dobricic et al. (2007), and \mathbf{B}_r contains the horizontal covariances and eigenvalues of vertical EOFs. Matrix \mathbf{B}_r is defined as

$$\mathbf{B}_r = \mathbf{\Lambda}^{1/2} \mathbf{C} \mathbf{\Lambda}^{1/2}, \quad (3)$$

where $\mathbf{\Lambda}^{1/2}$ is a diagonal matrix containing the singular values associated with each EOF and \mathbf{C} contains the horizontal covariance. In this particular implementation of SOFA, the horizontal covariances are Gaussian functions of distance with an e -folding radius of 60 km.

The EOFs are seasonally dependent, meaning that they have been calculated using the composite record for each season, and they are defined in each of the 13 geographical regions shown in Fig. 2. Twenty EOFs are kept for each region and season (Dobricic et al. 2005) and the remaining EOFs are considered to span the null space. The EOFs are quadrivariate, containing the covariance between surface elevation η , temperature T ,

salinity S , and barotropic streamfunction Ψ , defined as $\mathbf{u} = (1/H)\mathbf{k} \times \nabla\Psi$, where \mathbf{u} is the barotropic velocity field, H is the depth, and \mathbf{k} is the vertical unit vector. Formally the state vector may be written as $\mathbf{x} = [T, S, \eta, \psi]$; by using the singular value decomposition the state vector can be rewritten as $\mathbf{x} = \mathbf{\Sigma}\mathbf{\Lambda}^{1/2}\mathbf{P}^T$, where \mathbf{P} is the matrix of the right singular vectors, which contains the expansion coefficient of the EOFs. Corrections to the velocity fields are imposed after calculating corrections to T and S , using the geostrophic relationship as described by Dobricic et al. (2007). However, this formulation restricts the assimilation of the sea level anomaly (SLA) observations only in areas deeper than the level of no motion depth, which is chosen to be 1000 m. Corrections to the barotropic component of the velocity can generate fast barotropic gravity waves, and in order to reduce the impact of these waves a “divergence damping filter” is used (Talagrand 1972; Dobricic et al. 2007). The assimilation cycle is daily and uses the first-guess-at-appropriate-time (FGAT) method, as described in Dobricic et al. (2007).

The other assimilation scheme used in this paper is the three-dimensional variational method OceanVar, which iteratively finds the minimum of the cost function written as follows:

$$\mathbf{J}(\mathbf{x}) = \frac{1}{2}\{(\mathbf{x} - \mathbf{x}_b)^T \mathbf{B}^{-1}(\mathbf{x} - \mathbf{x}_b) + [\mathbf{H}(\mathbf{x}) - \mathbf{y}]^T \mathbf{R}^{-1}[\mathbf{H}(\mathbf{x}) - \mathbf{y}]\}, \quad (4)$$

where \mathbf{x} is the analyzed state vector, \mathbf{x}_b is the first guess or background state vector, \mathbf{y} is the observation vector, \mathbf{H} is the linearized observational operator, and \mathbf{B} and \mathbf{R} are the model background and observational error covariance matrices, respectively. The state vector is defined by $\mathbf{x} = [T, S, \eta, \mathbf{U}, \mathbf{V}]$, where T , S , η , \mathbf{U} , \mathbf{V} are the three-dimensional temperature, salinity, and zonal and meridional velocity fields, respectively. The cost function is minimized in the control space $\mathbf{g} = \mathbf{G}^+(\mathbf{x} - \mathbf{x}_b)$, where superscript “+” indicates the generalized inverse and matrix \mathbf{G} is a square root of \mathbf{B} :

$$\mathbf{B} = \mathbf{G}\mathbf{G}^T. \quad (5)$$

In OceanVar, the operator \mathbf{G} is modeled as a successive application of a set of linear operators

$$\mathbf{G} = \mathbf{G}_D \mathbf{G}_{UV} \mathbf{G}_B \mathbf{G}_H \mathbf{G}_V. \quad (6)$$

Here, \mathbf{G}_D is the divergence damping filter, \mathbf{G}_{UV} is the geostrophic balance relationship for the baroclinic components of velocity, \mathbf{G}_B is a barotropic model that links temperature and salinity increments with sea level and barotropic velocity, \mathbf{G}_H models horizontal

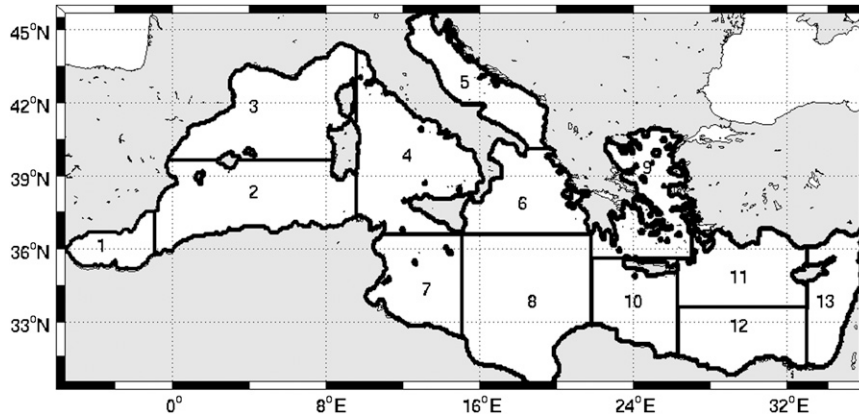


FIG. 2. Regions of the Mediterranean Sea.

covariances, and \mathbf{G}_V contains the same vertical EOFs multiplied with their singular values of SOFA, that is, $\mathbf{x} = \Sigma \Lambda^{1/2} \mathbf{P}^T$. On the other hand, in OceanVar, a barotropic model is used to calculate the correction to the sea surface height and barotropic velocities. The advantage of this formulation with respect to the simple geostrophic balance method used in SOFA is that the assimilation corrections can be calculated everywhere. We have chosen to assimilate only in regions deeper than 150 m; this depth in the Mediterranean ensures that satellite sea surface height is used only from approximately 50 km offshore. The major difference between the SO-RE and OV-RE experiments is, thus, the assimilation of satellite altimetry data, implying that the number of the assimilated observations is larger in OV-RE than in SO-RE.

c. Assimilated observations

The reanalyses use a comprehensive observational in situ and satellite dataset that includes

- satellite SST data,
- in situ temperature and salinity profiles, and
- satellite SLA from altimetry.

SST satellite observations are time series of maps interpolated on the model grid. The data available from 1985 to 2005 are reanalyzed optimal interpolated SST (OISST; Marullo et al. 2007), while from 2006 the delayed-time dataset is used, which has been produced following the procedure of Buongiorno Nardelli et al. (2003) but uses as a final grid the same grid as the OGCM presented above.

The in situ dataset is built on the historical data archive of MedAtlas (Maillard et al. 2005), and it contains vertical profiles of temperature and salinity from bottles, thermometers, XBT, mechanical bathythermograph (MBT),

and CTD sensors. Only the profiles that have the best-quality flag have been used for the assimilation. The MedAtlas dataset spans the period from 1985 to 1999, and has been merged with the data from the Ship-of-Opportunity Program (Manzella et al. 2007) and the MedArgo program (Poulain et al. 2007) for the subsequent period. In Table 2 the number of in situ observations as a function of reference regions (Fig. 2) and years is shown. We anticipate that the lack of sampling homogeneity in space and time and the significant difference in the number of observations in different subperiods will be a major drawback in the quality of the reanalyses. This discussion will be addressed more specifically in section 4.

The satellite SLA measurements are taken from *European Remote Sensing Satellite (ERS)-1*, *ERS-2*, *Environmental Satellite (Envisat)*, *Ocean Topography Experiment (TOPEX)/Poseidon*, and *Jason-1* satellite missions. These data and relative corrections are described by Pujol and Larnicol (2005). Once again, the satellite observations have been subdivided by region, and the number of SLA measurements as a function of years and regions is shown in Table 2. To compute the SLA from the model, the mean dynamic topography (MDT) is subtracted from the model SSH. The MDT is estimated successively by correcting the estimate by Rio et al. (2007) with unbiased estimates from in situ observations used in the operational assimilation system. The methodology to correct MDT by unbiased in situ observations is described in Dobricic (2005).

3. Reanalysis intercomparison

In this section we present the intercomparison between OV-RE, SO-RE, and SIM. The forcing used is the same for all three numerical experiments, but because the fluxes are computed interactively they change between the three experiments.

TABLE 2. Number of temperature, salinity profiles, and sea level anomaly observations assimilated by OceanVar for each year and region.

	Reg 1	Reg 2	Reg 3	Reg 4	Reg 5	Reg 6	Reg 7	Reg 8	Reg 9	Reg 10	Reg 11	Reg 12	Reg 13
Temperature													
1985	364	437	282	312	98	187	56	254	190	134	328	231	388
1986	629	634	644	1399	155	632	309	1349	314	309	307	156	161
1987	309	542	597	1125	214	244	110	401	314	224	229	227	54
1988	153	339	440	358	41	186	86	264	391	777	536	377	30
1989	125	360	398	360	222	135	55	253	191	111	235	87	163
1990	218	559	308	283	403	167	74	305	222	78	160	105	53
1991	303	304	504	92	248	66	34	155	85	81	158	69	63
1992	171	249	563	93	443	31	46	52	25	59	91	55	7
1993	120	225	536	137	545	238	49	121	63	84	168	382	312
1994	87	43	363	11	490	190	1	2	77	13	7	37	0
1995	28	114	656	51	1108	66	1	9	130	16	53	5	35
1996	62	37	172	1	267	14	0	0	79	0	71	11	66
1997	217	39	251	6	135	1	22	8	117	0	22	0	26
1998	19	66	80	4	291	11	0	2	80	30	49	30	4
1999	56	229	262	214	113	173	5	39	58	101	137	151	21
2000	91	445	461	635	202	248	15	127	138	109	297	311	26
2001	0	0	0	0	56	78	0	35	0	0	35	0	0
2002	0	0	22	0	128	206	0	73	0	0	91	8	0
2003	0	0	35	0	250	184	0	72	0	30	178	52	204
2004	8	174	299	351	0	75	14	92	88	38	333	195	297
2005	19	208	364	566	52	278	30	299	88	155	479	306	189
2006	47	119	153	206	192	111	2	218	65	308	176	244	147
2007	20	123	220	200	76	52	121	234	7	221	157	78	135
Salinity													
1985	246	65	132	97	85	34	28	26	87	12	46	38	14
1986	500	157	220	109	143	21	14	17	99	24	105	6	4
1987	13	59	339	267	207	26	22	27	171	32	56	7	7
1988	23	57	288	192	37	44	18	33	120	26	30	15	1
1989	10	82	97	144	213	20	26	61	97	30	46	11	2
1990	75	168	240	122	391	66	53	54	145	10	45	16	0
1991	272	125	352	21	251	22	1	22	35	7	35	4	0
1992	161	205	549	52	398	21	31	13	3	0	0	0	4
1993	103	149	486	80	290	0	0	0	31	4	12	7	40
1994	82	35	333	0	433	167	0	0	57	11	4	30	0
1995	28	84	648	49	1102	64	1	9	93	16	53	5	35
1996	62	13	152	0	259	10	0	0	57	0	71	11	65
1997	205	5	129	0	134	0	0	0	103	0	21	0	26
1998	18	64	80	0	285	0	0	0	46	0	0	0	0
1999	3	8	140	4	5	2	2	2	3	34	0	0	0
2000	0	0	46	0	10	0	0	0	0	0	0	0	0
2001	0	0	0	0	0	0	0	35	0	0	35	0	0
2002	0	0	0	0	0	0	0	72	0	0	91	8	0
2003	0	0	35	0	0	0	0	72	0	30	165	39	194
2004	0	46	121	61	0	33	0	55	0	14	200	97	217
2005	19	119	230	157	0	99	0	189	10	70	277	118	115
2006	46	95	142	89	1	28	0	176	65	300	166	230	147
2007	0	83	139	64	0	0	42	181	7	209	149	78	135
Sea level anomaly													
1992	231	1243	1034	849	179	662	671	1932	182	651	774	757	333
1993	1537	9321	8312	6320	1312	4765	5429	14229	1550	4663	6623	5718	3718
1994	577	4698	4923	3462	754	2546	2846	7615	973	2171	3469	2816	2447
1995	1362	8625	8451	6375	1448	4259	5258	11912	2568	4344	6251	5112	3880
1996	1615	10056	9837	7442	1839	5064	5970	13455	2797	5050	7321	5979	4328
1997	1630	10281	9702	7262	1877	5386	5893	13671	2844	5061	7428	6106	4259
1998	1629	10162	9808	7239	1945	5237	5809	13309	2713	4900	7262	6123	4153
1999	1646	10592	10169	7160	1987	5535	5789	13602	2791	5153	7401	6258	4350
2000	1664	10188	9894	6804	1930	5200	5741	13334	2730	4976	7138	5989	4359

TABLE 2. (Continued)

	Reg 1	Reg 2	Reg 3	Reg 4	Reg 5	Reg 6	Reg 7	Reg 8	Reg 9	Reg 10	Reg 11	Reg 12	Reg 13
2001	1517	9716	9422	6773	1785	5065	5621	13298	2601	4802	6892	5675	3991
2002	1677	10268	9764	7206	1886	5181	5860	13442	2830	4958	7304	5926	4393
2003	1568	9761	9591	6892	1617	4635	5581	12818	2575	4736	7043	5590	4429
2004	1701	9874	9397	8463	2034	4660	5706	11988	5081	5096	7815	6214	4757
2005	1515	10041	9567	8308	2024	4778	5837	12183	5043	5132	8251	6431	4784
2006	1651	9826	9451	7976	2134	4775	5607	12135	4743	4986	8111	6254	4791
2007	1506	10049	9587	8305	2082	4772	5952	12394	4588	5110	8152	6416	4900

a. Surface atmospheric fluxes

We start our discussion by looking at the basin-averaged forcing in all of the experiments and comparing it with a climatology calculated from the corrected ERA-40 fluxes (Pettenuzzo et al. 2010). The long-term mean value for this period is $-0.4 \pm 1.5 \text{ W m}^{-2}$ for SIM, $1.8 \pm 1.5 \text{ W m}^{-2}$ for OV-RE, and $0.7 \pm 1.5 \text{ W m}^{-2}$ for SO-RE. Pettenuzzo et al. (2010) estimates that the uncertainty in the long-term mean surface heat flux is $\pm 3 \text{ W m}^{-2}$; thus, all three numerical experiments produce a similar surface heat balance within uncertainty errors. The values are somewhat positive with respect to the well-known negative heat flux budget of the Mediterranean Sea ($-6 \pm 3 \text{ W m}^{-2}$), but we argue that this depends on the specific time period used, as explained in Pettenuzzo et al. (2010).

The period of 1985–2000 coincides with a positive North Atlantic Oscillation (NAO) period (Hurrell et al. 2001), and values are expected to be above the long-term average.

The basin mean water flux of Fig. 3 shows a strong seasonality with a maximum in autumn and a minimum in spring. The interannual mean values are 600 mm yr^{-1} for OV-RE and SO-RE and 670 mm yr^{-1} for SIM. The river’s contribution accounts for 70 mm yr^{-1} , and the Dardanelles’ for about 130 mm yr^{-1} .

The climatological interannual mean value computed for the period of 1985–2001 given by Pettenuzzo et al. (2010) is 700 mm yr^{-1} , not taking into account either the river’s or Dardanelles’s water input. Excluding these two sources of freshwater from the reanalysis, the water budget rises to 800 mm yr^{-1} . Thirty percent of this difference

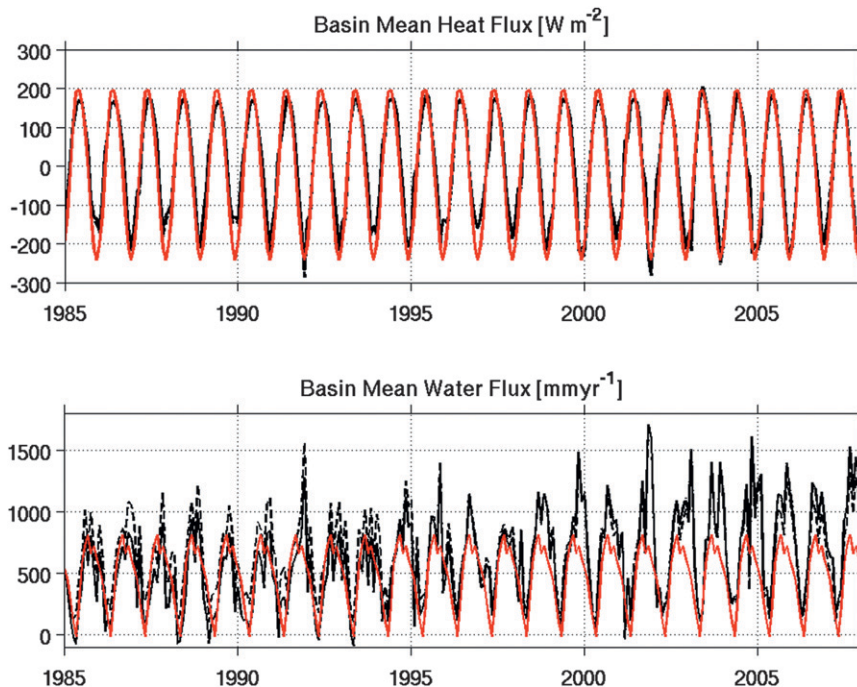


FIG. 3. Time series of (top) Mediterranean basin mean heat flux (W m^{-2}) and (bottom) water flux (mm yr^{-1}). In both panels, climatology (red curves), OV-RE (continuous lines), SO-RE (dashed-dotted lines), and SIM (dashed lines) are shown.

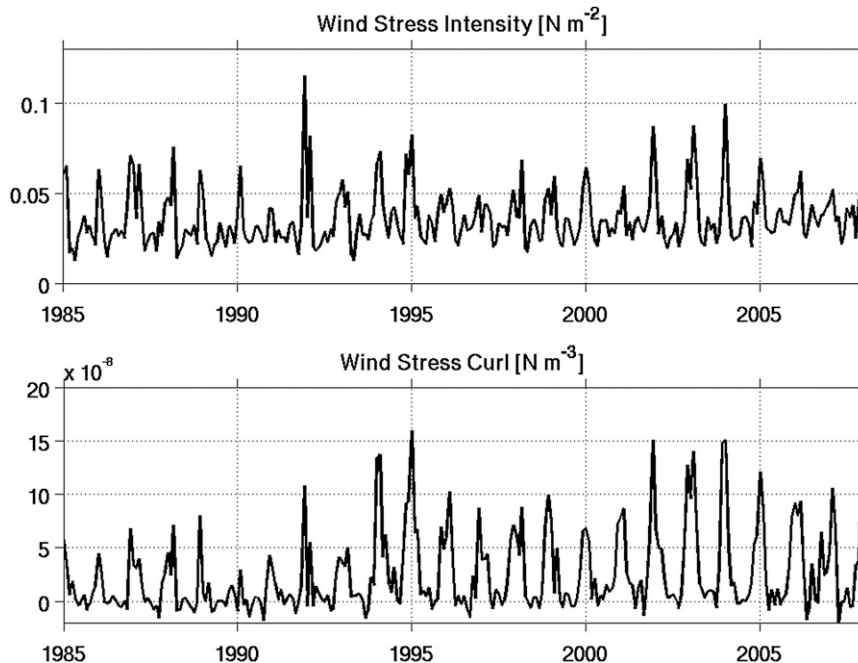


FIG. 4. Time series of (top) Mediterranean basin mean wind stress intensity and (bottom) the vertical component of the wind stress curl.

is due to the different precipitation datasets, while the remaining 70% is due to evaporation. We argue that this last difference mainly results from the different wind and humidity datasets between the two papers, as well as from the different time period taken into account. All of the experiments show an increasing tendency in the basin mean evaporation; this difference can be explained by the changes that occurred in the wind field during the study period, as shown in Fig. 4. The wind stress intensity changes from an average value of 0.034 N m^{-2} before 1995 to 0.037 N m^{-2} after. The increase is partly due to a change in the atmospheric forcing resolution, but also the interannual variability of the forcing, as explained in Pettenuzzo et al. (2010).

b. Sea surface and volume temperature

The intercomparison of SST for the three experiments is shown in Fig. 5. It is evident that a low-frequency climate variability signal is superimposed on a large seasonal cycle and that interannual anomalies are present both in winter and summer [notice the large summer 2003 anomaly (see Olita et al. 2007)]. Both SO-RE and OV-RE give the same SST estimates as a consequence of the surface relaxation term. The SST differences between SIM and the reanalyses are evident in the period of 1985–94, probably because of the inaccuracies of the ERA-15 forcing. SIM is generally warmer than the reanalyses. The two

reanalyses give a positive trend of $0.1^\circ\text{C yr}^{-1}$, unlike SIM, which shows a $-0.03^\circ\text{C yr}^{-1}$ negative trend. Averaged satellite SST observations give a positive $0.03^\circ\text{C yr}^{-1}$ trend, in agreement with the reanalyses.

It is interesting to notice that even though the surface heat flux and the net heat transport through the Strait of Gibraltar (not shown) are similar between SIM and the reanalyses, the basin mean temperatures are quite

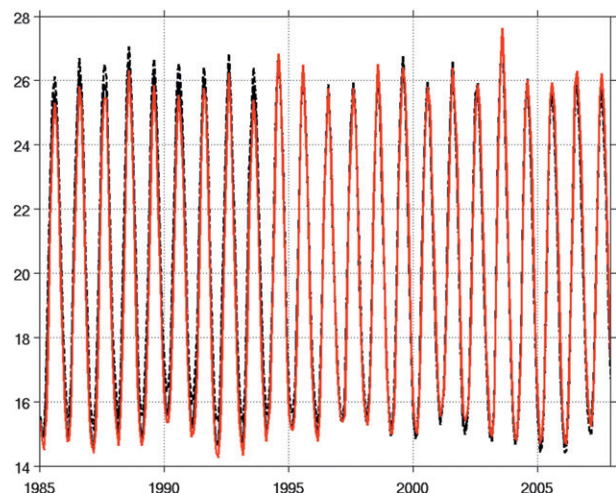


FIG. 5. Time series of mean sea surface temperature for satellite observations (red line), SIM (black dashed line), and OV-RE (black continuous line) experiments.

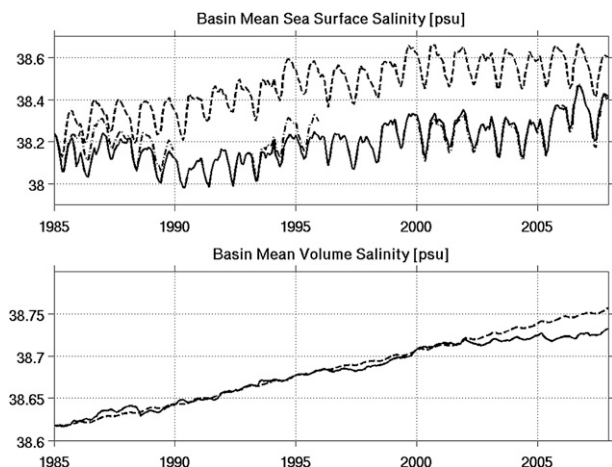


FIG. 7. Time series of (top) mean sea surface salinity for SO-RE (dot-dashed line), OV-RE (continuous line), and SIM (dashed line), and (bottom) mean volume salinity.

not a clear trend: surface salinity seems more driven by interannual variability, with quite an evident shift toward higher values in January 1994 and 1999 and in spring/summer 2005. We argue that this behavior is primarily forced by the increase of evaporation occurring in these years related to the increase in wind speed.

The bottom panel of Fig. 7 shows the mean volume salinity for OV-RE and SIM; the SO-RE solution is

omitted because the solution is indistinguishable from OV-RE. There is a clear positive trend for the first 16 yr; however, from 2000 to 2007 the two experiments diverge. SIM continues a linear trend while OV-RE becomes flat. The whole time series trend for SIM is about 6×10^{-3} psu yr $^{-1}$, while for OV-RE it is 5×10^{-3} psu yr $^{-1}$.

d. Vertical distribution of temperature and salinity

Because the SSS and SST time series behavior is different from the volume-averaged values, it is interesting to investigate how the salinity and the temperature are distributed along the water column. The vertical distribution of the temperature and salinity anomalies, when compared to the MedAtlas climatology (Maillard et al. 2005), is shown in Figs. 8 and 9.

In the mixed layer, down to 50 m, the temperature anomalies show an alternation of positive and negative anomalies, indicating that the seasonal cycle in the reanalyses is more pronounced than that in the climatology. The winters are slightly colder than the climatology and the summers are warmer, exceeding the amplitude of the seasonal cycle computed by the observed climatology. However, it has to be kept in mind that, while the reanalysis data are almost continuous in space and time, the observed climatology was made out of sparse observations. Overall there is a warm bias in the first 100 m

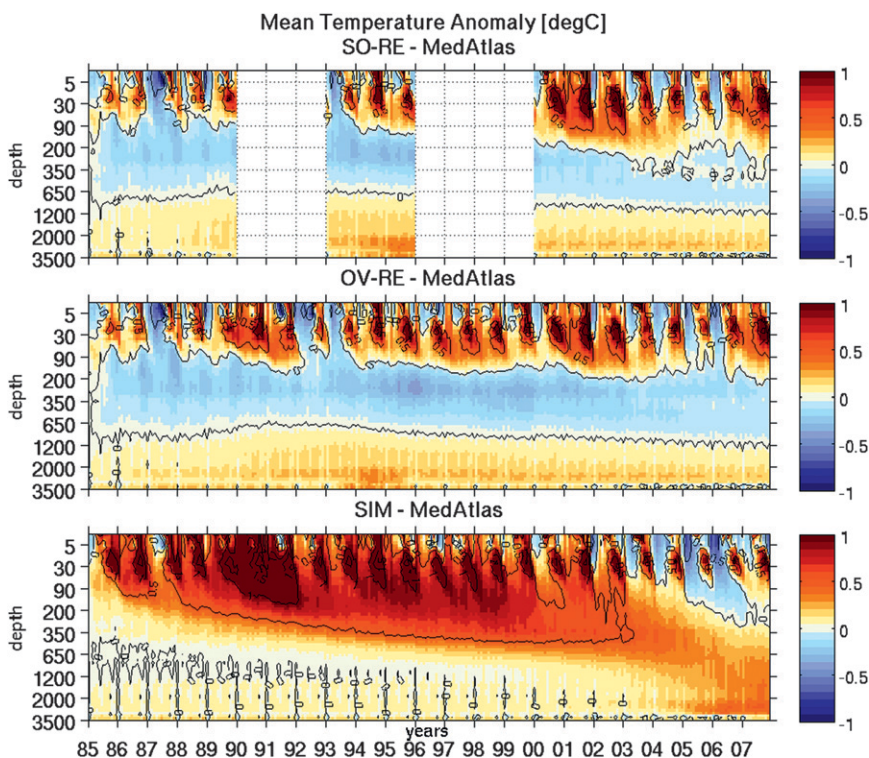


FIG. 8. Basin mean temperature anomalies with respect to MedAtlas climatology.

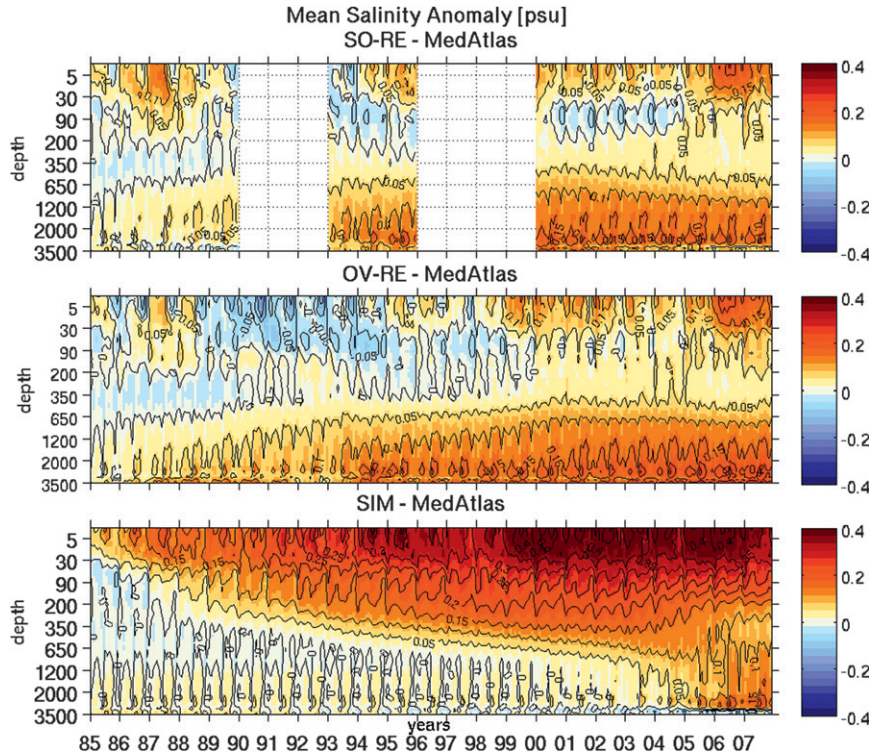


FIG. 9. Basin mean salinity anomalies with respect to MedAtlas climatology.

and a cold one between 100 and 900 m, which is stronger in OV-RE than in SO-RE. In the bottom layers, from 900 m downward, the temperature increases, more in OV-RE than in SO-RE. Also noticeable is the warm event at 3000 m in the years of 1993–95, which is probably due to the eastern Mediterranean transient (EMT; Roether et al. 1995; Gertman et al. 2006), which is visible in both the SO-RE and OV-RE. EMT corresponds to an increase of salinity in the bottom of the Levantine Basin resulting from a shift in the location of deep-water formation from the Adriatic to the Aegean Sea, which implied a change in thermohaline circulation (Roether et al. 1995; Gertman et al. 2006). The vertical distribution of SIM temperature anomalies, however, shows a large warm bias deepening in the water column up to 2003. This is a model drift that is somewhat halted after 2005, when cooling occurs because of atmospheric forcing.

The salinity anomalies of Fig. 9 show the same pattern again for SO-RE and OV-RE: the interannual anomalies are positive in the upper and lower water column, while between 100 and 700 m they are negative. Once again, positive deep-water salinity anomalies occur after 1993, which is the start of the mature phase of the EMT. On the other hand, the SIM salinity starts to increase in the upper water column from the beginning of the experiment, and then it spreads to intermediate and

bottom depths, where it is trapped. We believe this is a drift of the model simulation that is partly corrected by the assimilation.

This comparison with climatology has shown for the first time that data assimilation schemes, such as SOFA and OceanVar, are capable of partially correcting for water mass property drifts, even if biases connected to model errors, which are not yet properly considered in the assimilation scheme, are still present.

e. Sea surface height

Finally, we conclude the intercomparison by showing the basin mean SSH for SIM, OV-RE, and SO-RE in Fig. 10. Small differences are found between the experiments and are concentrated in the first 7 yr. The OV-RE and SO-RE solutions are closer after 1992, as expected, because both started to assimilate satellite SLA. The SSH has a clear seasonal cycle of about 5 cm with large interannual variability.

4. Assessment of the reanalysis quality

To quantitatively assess the reanalysis, we have evaluated statistics on the misfits defined as follows:

$$\mathbf{m} = -[\mathbf{y}_o - \mathbf{H}(\mathbf{x})],$$

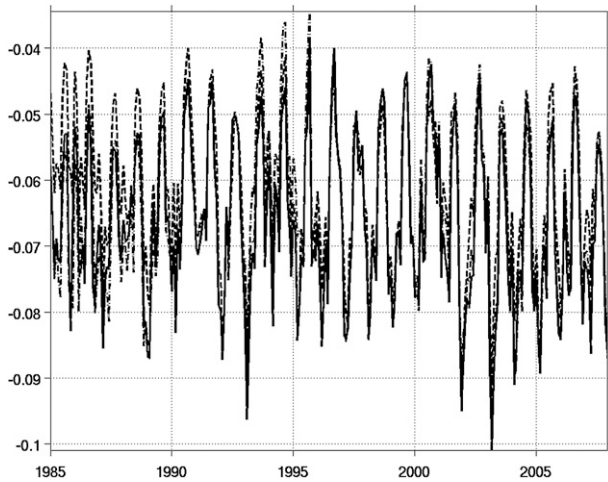


FIG. 10. Time series of basin mean sea surface height for SIM (dashed line), OV-RE (continuous line), and SO-RE (dashed-dotted line).

where y_o is the observation, \mathbf{H} is the linearized observational operator, and \mathbf{x} is the model solution. Misfits have been computed using the background model fields before the data are inserted so that observations are

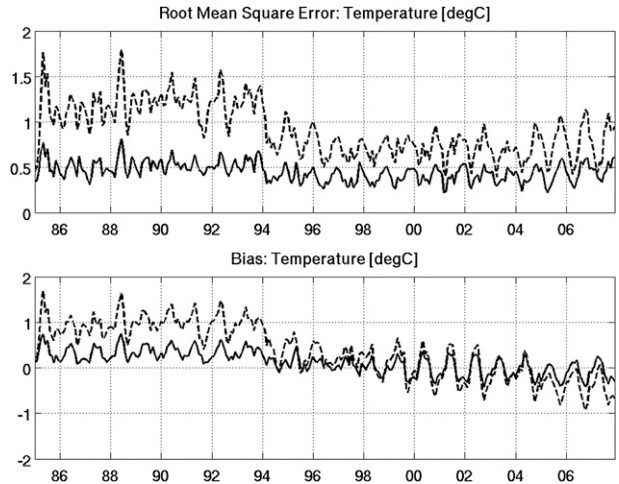


FIG. 11. (top) RMSE and (bottom) bias for SST. OV-RE (continuous line) and SIM (dashed line) are shown in both panels.

fully independent. However, it has to be kept in mind that close observations in either space or time may be correlated to each other by creating a weak dependence between the background and the observations while the

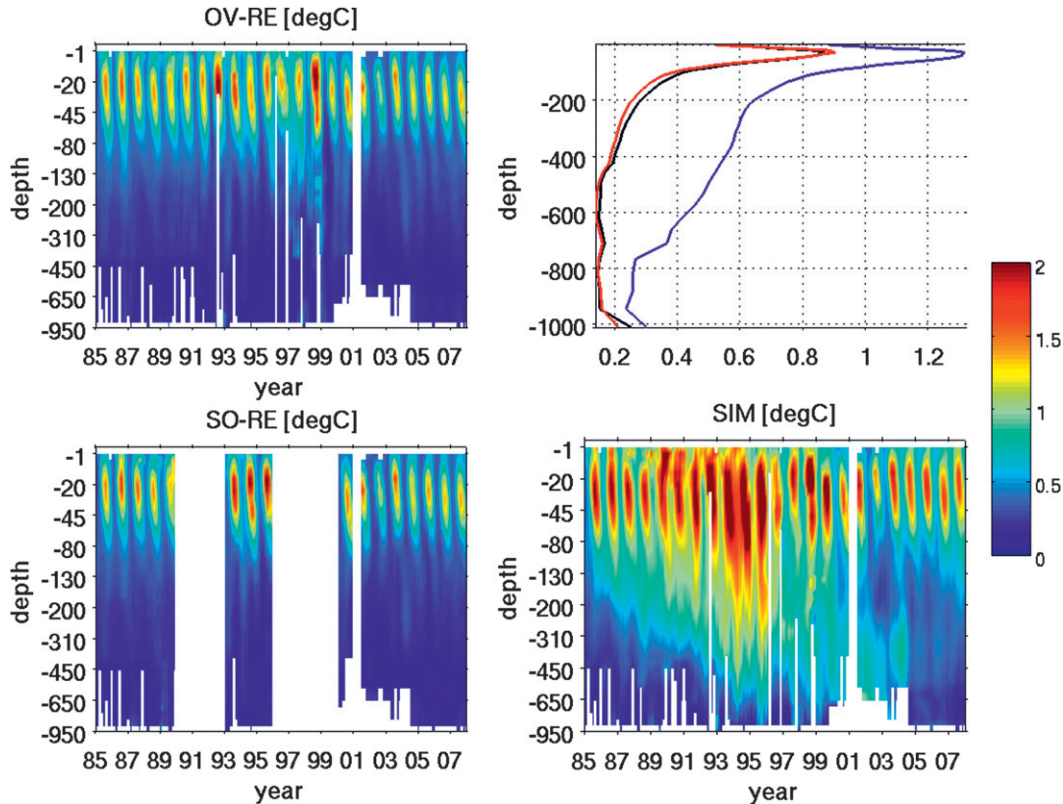


FIG. 12. Temperature RMSE as function of time and depth for (top left) OV-RE, (bottom left) SO-RE, and (bottom right) SIM. (top right) Time mean temperature RMSE as function of depth is shown for SIM (blue line), SO-RE (red line), and OV-RE (black line).

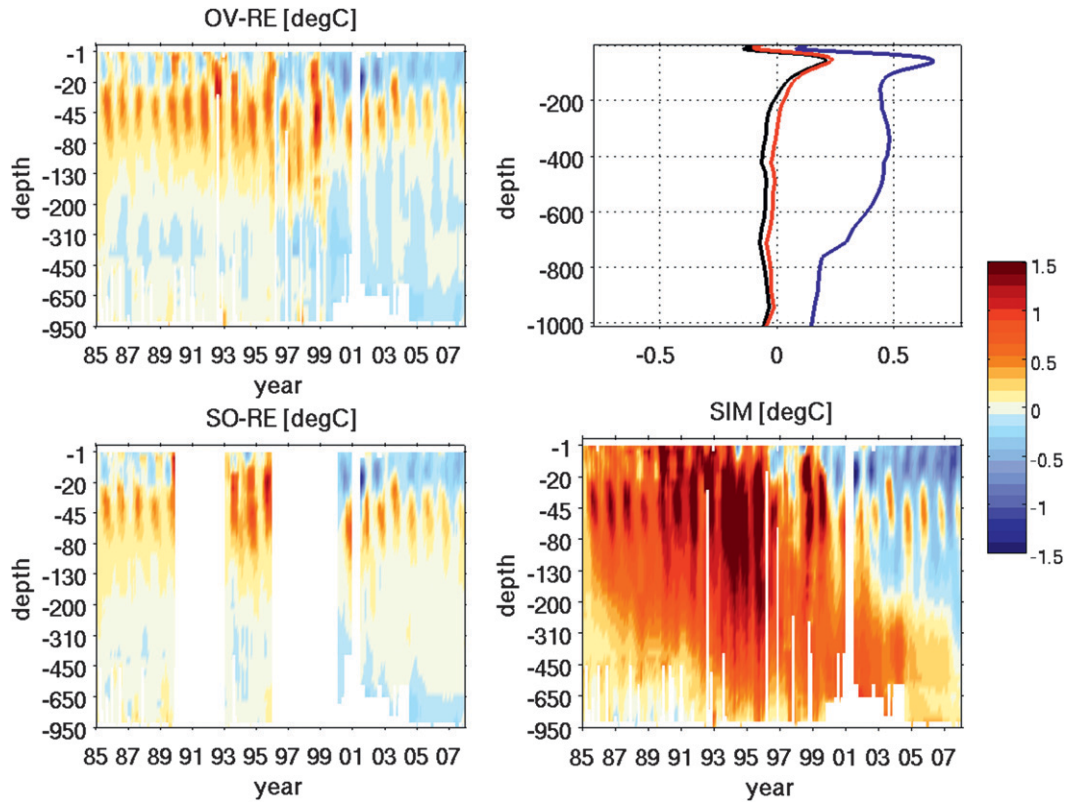


FIG. 13. Temperature bias as function of time and depth for (top left) OV-RE, (bottom left) SO-RE, and (bottom right) SIM. (top right) Time mean temperature bias as function of depth for SIM (blue line), SO-RE (red line), and OV-RE (black line).

latter are assimilated. This is particularly true because most of our data are sparse in space and time, so we can consider the background to be unaffected by observations assimilated previous to the current time. CTD datasets from 1985 to 1999 have been collected from research cruises in the Mediterranean Sea, which were carried out in various regions, so that the computed misfits give an estimate of the model error. Argo floats have a surfacing period of 5 days (Poullain et al. 2007) and travel several tens of kilometers between surfacing points, thus making a comparison with one profile that is almost independent from the previously assimilated profile.

The only dependent dataset that we will use to assess the quality of the reanalysis is the satellite SST because the model is relaxed to the observed SST every day. Thus, differences between satellite SST and SO-RE and OV-RE are not independent, while SIM differences are. The SST root-mean-square error (RMSE) and bias is shown in Fig. 11. From 1985 to 1994 the simulation RMSE is about 1.3°C, decreasing to 0.7°C when the forcing fields increase the resolution after 1995. After 1995 a clear RMSE seasonal cycle is visible, indicating a greater error during spring. The SST RMSE for SIM

increases again after 2005 when we changed from re-analyzed SST (Marullo et al. 2007) to analysis products (Buongiorno Nardelli et al. 2003). OV-RE and SO-RE RMSE are identical, as expected, and they show a mean RMSE of about 0.5°C with a slight decrease after 1994. An RMSE of 0.5°C is also intrinsically present in the OI-SST product because of the optimal interpolation procedure, as mentioned in Marullo et al. (2007), meaning that only part of this error is due to OV-RE and SO-RE. These results show that errors are larger during spring and summer than in winter, which is probably due to the inaccurate parameterization of heat penetration in the water column, in addition to forcing errors.

In the bottom panel of Fig. 11 the SST misfit bias is shown: the SIM SST is warmer than the observations in the first 11 yr (by about 1°); from 1996 to 2004 the annual mean bias is almost zero; and for the last 3 yr the bias becomes negative, indicating a colder model SST than that observed. The OV-RE and SO-RE solutions also show the same trend, even though it is reduced when compared to SIM. This bias is due to the inaccuracies of the forcing, which is the same in the SIM and the data assimilation experiments.

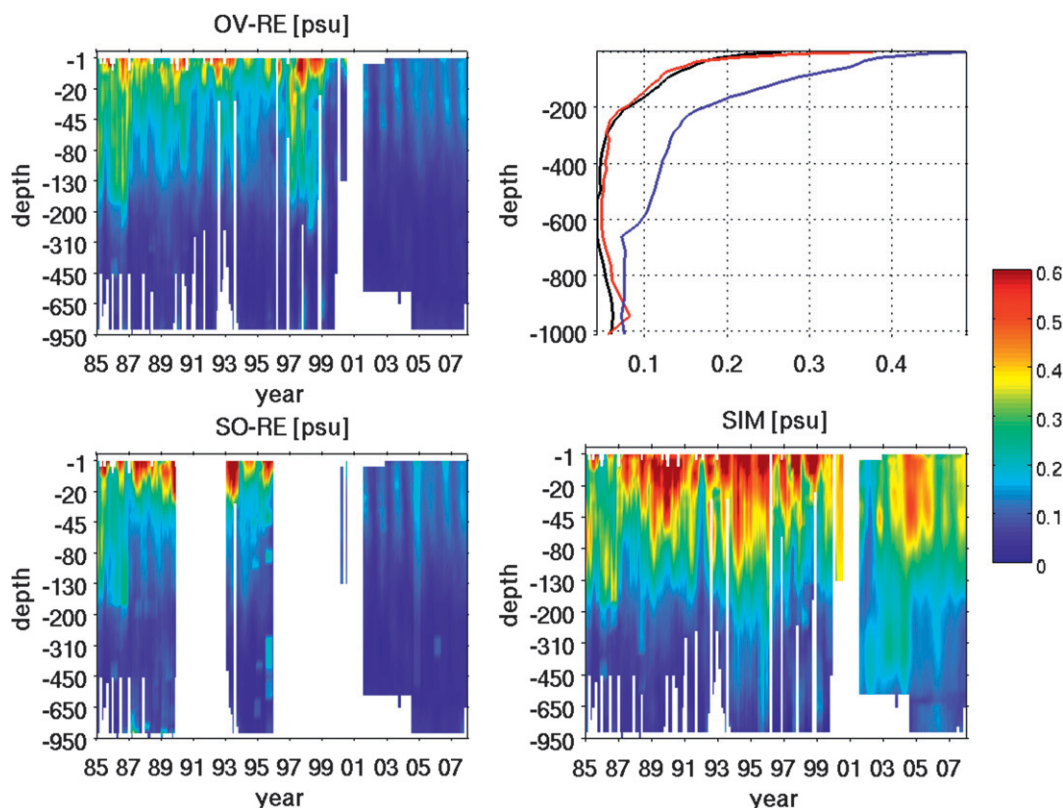


FIG. 14. Salinity RMSE as function of time and depth for (top left) OV-RE, (bottom left) SO-RE, and (bottom right) SIM. (top right) Time mean salinity RMSE as function of depth for SIM (blue line), SO-RE (red line), and OV-RE (black line).

The RMSE and bias of the temperature and salinity profile misfits are presented in Figs. 12–15. The temperature RMSE and bias for the three experiments are presented in Figs. 12 and 13. The reanalysis RMSE is lower than the simulation for both SO-RE and OV-RE, but the error structure is similar: the maximum error is achieved at the base of the mixed layer depth, at about 30 m, and it is seasonal, with the highest values in summer and the lowest in winter, which is related to the inadequate representation of the upper-thermocline formation processes. This error is partly due to the uncertainties in the wind forcing (Milliff et al. 2011, manuscript submitted to *Quart. J. Roy. Meteor. Soc.*; Bonazzi et al. 2011, manuscript submitted to *Quart. J. Roy. Meteor. Soc.*) and the model-mixing parameterizations (appendix A), as well as the advective processes that bring Atlantic Modified Waters (AMW) from the Strait of Gibraltar to different locations throughout the Mediterranean Sea. The large error in 1994–95 in SIM is due to inaccurate representation of the EMT in the simulation alone. The assimilation experiments instead used the Physical Oceanography of the Eastern Mediterranean (POEM) dataset (Malanotte-Rizzoli et al. 1999), and the error is reduced in 1993–95.

The average error in the first 100 m is 0.6°C , from 100 to 500 m it is 0.3°C , and from 500 m to the bottom it is less than 0.2°C for SO-RE and OV-RE. For SIM the same values are 1° , 0.6° , and 0.4°C for the first 100 m, from 100 to 500 m, and from 500 m to the bottom, respectively.

The bias estimates (Fig. 13) for SO-RE and OV-RE are comparable, as was the case with RMSE, while SIM exhibits quite a large warm bias all through the water column with a maximum in the early 1990s changing to a cold bias starting from 2000. Both warm and cold biases start to develop at the surface and then tend to deepen along the water column. The maximum bias error is centered at the depth of 60 m for both the reanalysis and SIM, where the subsurface minimum of salinity corresponding to MAW resides (Pinardi et al. 2006). However, the maximum bias values occupy a wider interval of depths than the RMSE, highlighting the water in the thermocline as being too warm and again pointing to the wind forcing uncertainties as possible sources of the errors.

Figures 14 and 15 show the RMSE and the bias for salinity, respectively. The maximum RMSE in salinity is

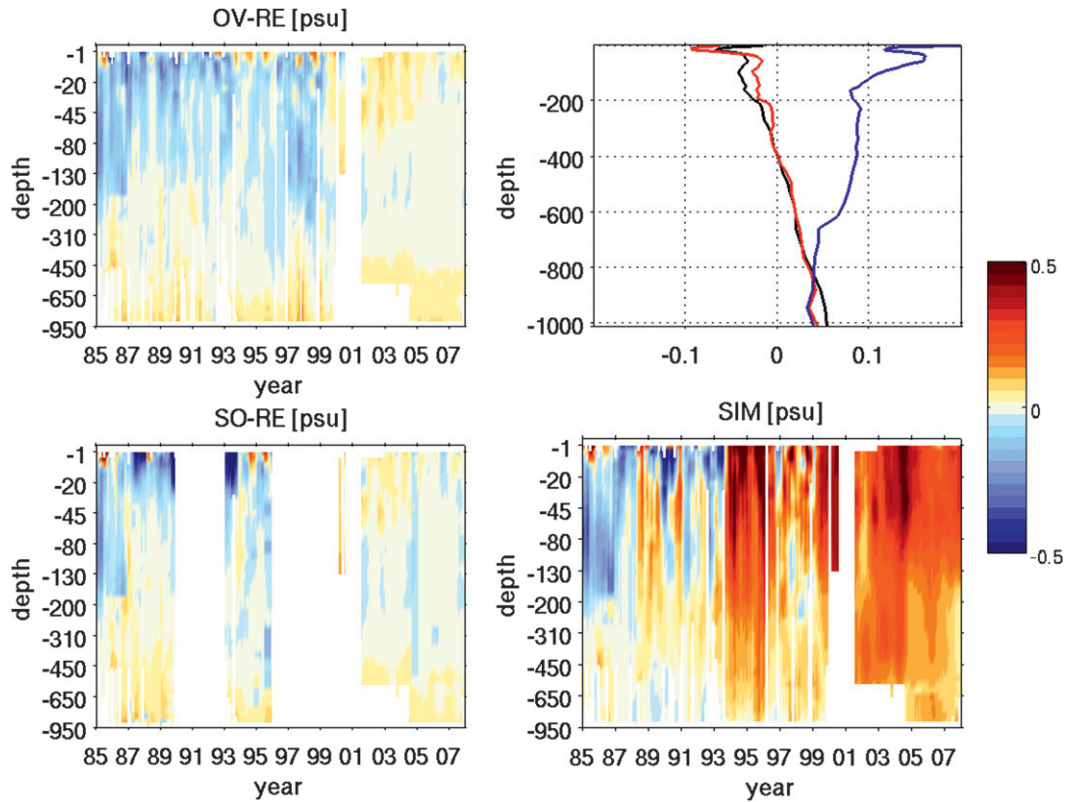


FIG. 15. Salinity bias as function of time and depth for (top left) OV-RE, (bottom left) SO-RE, and (bottom right) SIM. (top right) Time mean salinity bias as function of depth for SIM (blue line), SO-RE (red line), and OV-RE (black line).

at the surface and it halves around 80 m; OV-RE and SO-RE show smaller RMSE than SIM. It is worth emphasizing that bias and RMSE have almost the same values, indicating that the systematic error in salinity is as big as the RMSE. The model in all three experiments is fresher than the observations at the beginning of the numerical experiment period, and then it changes. For OV-RE the change appears in 2000, while for SIM the change occurs in 1994 when the resolution of the atmospheric forcing doubles.

It is evident in the RMSE and bias that the salinity error decreases significantly after 2000. To discern whether the model has better skill in reproducing the Mediterranean dynamics and water mass distributions after 2000, or if such improvement is artificially caused by the significant difference in the number of observations in the post-2000 period, the assimilated observations have been split into two datasets, pre-2000 and post-2000, which are shown in Fig. 16. The pre-2000 dataset is almost completely based on observations coming from the MedAtlas dataset, while the latter, from 2000 to 2007, comes from the Mediterranean Forecasting System (MFS) dataset (Pinardi et al. 2003).

The salinity profiles in the post-2000 period have increased by an order of magnitude resulting from the start of the MedArgo program (Poulain et al. 2007). Figure 16 shows that the reason is probably due to a combination of more abundant observations and better model skill, even though post-2000 abundance of profiles appears to be a dominant factor. Figure 16 shows that water mass changes are present between pre- and post-2000 years: the mean temperature and salinity profiles show a significant warming and increase of salinity between 200- and 400-m depths occurring in the post-2000 period. However, the spatial data distribution is so different for salinity pre- and post-2000 that the problem could be simply associated with a different sampling of water masses resulting from the different data sampling.

The seasonality of the errors coincides especially for the SST and the temperature profiles. The largest errors appear during summer both for the SST and the temperature profiles. The wrong formation of the summer thermocline correlates with the SLA error (Fig. 17). The error is most likely caused by model difficulties in reproducing the shallow summer of the Mediterranean

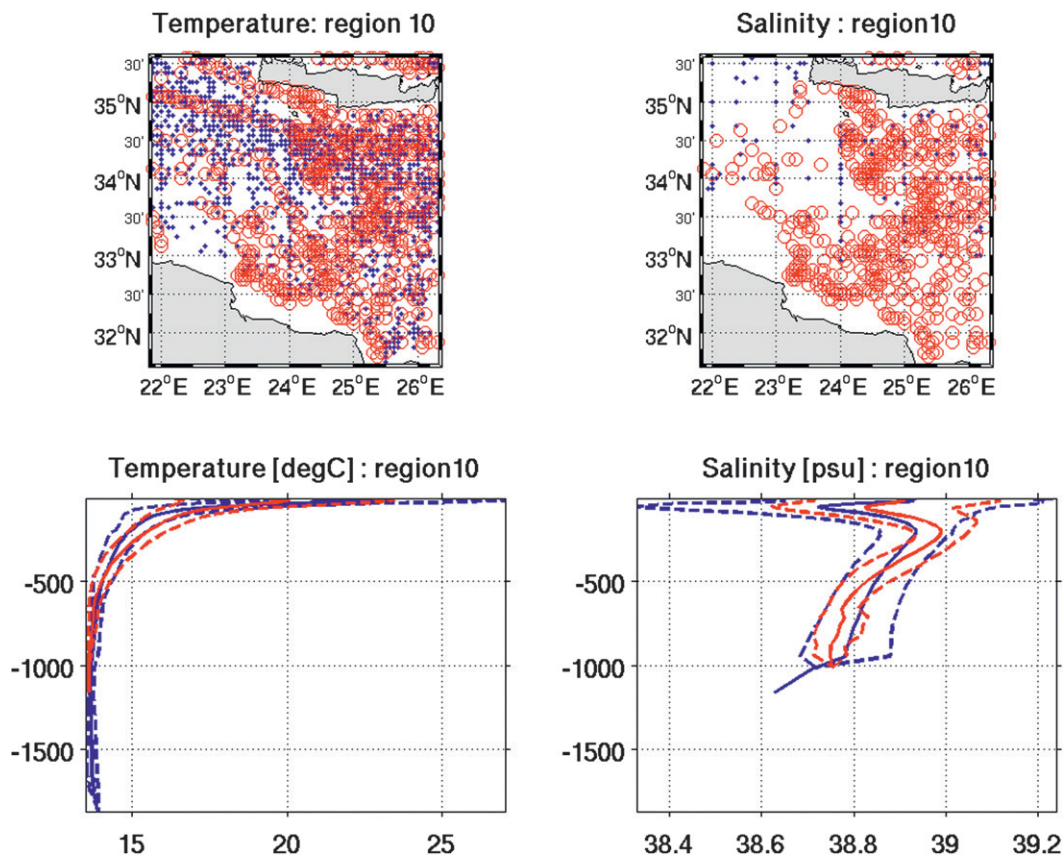


FIG. 16. Spatial distribution of (top left) temperature and (top right) salinity assimilated profile by OV-RE. (bottom left) Mean temperature and (bottom right) salinity profiles (continuous lines) \pm one standard deviation (dashed lines) are shown. Pre-2000 dataset (blue) and post-2000 dataset (red) are shown.

Sea resulting from insufficient upper water column vertical resolution and the limitation of the Pacanowski and Philander (1981) mixing scheme.

As a last quality assessment result, the RMSE for sea level anomaly (SLA) misfits is analyzed in Fig. 17. We would like to point out that the satellite dataset is quite an independent dataset because the minimum revisit time for all satellites is 10 days and tracks do not come one after the other in nearby positions. SIM time mean RMSE is approximately 6.5 cm with large interannual and seasonal variability. Here, OV-RE has lower RMSE than SO-RE probably because of the larger number of SLA data assimilated in OV-RE. As mentioned in section 2, SO-RE only assimilated the SLA observations in areas deeper than 1000 m and OV-RE in areas deeper than 150 m; this results in about 12% less SLA data assimilated by SO-RE than OV-RE.

Figure 18 shows the spatial distribution of time mean SLA RMSE. To compare the same years, RMSE has been computed for the period of 2000–07. Assimilation decreases the error almost everywhere with respect to the simulation, but the two areas of errors remain in the

reanalysis—one located in the Algerian basin (from 0° to 10° E) and the other southeast of Crete, Greece. Both areas are characterized by very high mesoscale variability (Pinaridi et al. 2006) and semipersistent gyres changes (Pujol and Larnicol 2005).

5. Discussion and conclusions

This study describes the quality and the overall consistency of two high-resolution reanalyses for the entire Mediterranean Sea which were performed by changing only the assimilation scheme. All of the available in situ and satellite information for the past 23 yr has been used with two assimilation schemes, a reduced-order optimal interpolation scheme (SOFA) and a three-dimensional variational scheme (OceanVar).

Three experiments have been intercompared: the two reanalyses SO-RE and OV-RE, and a simulation experiment SIM.

The first part of this study showed consistency in the heat and water budgets with respect to the climatological estimates of Pettenuzzo et al. (2010). Consistency has

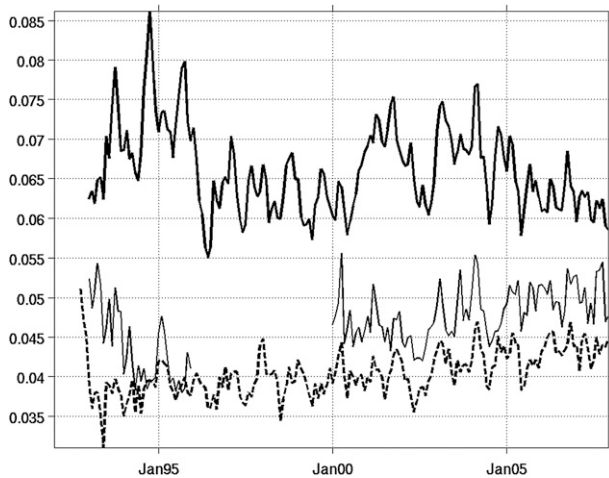


FIG. 17. RMSE as function of time for SLA. SIM (continuous thick line), SO-RE (continuous thin line), and OV-RE (dashed line).

also been found between the time series of SST, SSS, volume mean salinity and temperature, and profiles with respect to the MedAtlas climatology. We have shown that both assimilation schemes play an important role in redistributing the properties along the water column, correcting part of the deficiencies related to the ocean model and forcing inaccuracies.

The second part of the paper is dedicated to the study of the RMSE and bias errors computed from the misfits. This study shows that both assimilation schemes are capable of reducing the bias and root-mean-square errors with respect to the simulation, but that OV-RE improves the accuracy, especially for sea level. The largest RMSE and bias errors appear at the base of the summer–autumn mixed layer, and are probably connected to the atmospheric forcing uncertainties as well as inadequate model mixing parameterizations.

Temperature RMSE ranges from about 0.9° to 0.3°C in the first 200 m and from 0.3° to 0.1°C below, while bias is about 0.2°C in the first 200 m and 0.05°C below for SIM and OV-RE, respectively. Salinity RMSE ranges from 0.26 to 0.08 psu in 200 m and 0.05 psu below, while bias ranges from -0.05 to -0.02 psu in the first 200 m and from -0.01 to 0.05 psu below for SIM and OV-RE, respectively. Salinity bias errors decrease after 2000 in both the OV-RE and SO-RE results because of the start of the Argo data assimilation.

OV-RE gives better results for abundant data such as SLA, improving the RMSE by about 10% with respect to SO-RE, but giving the same RMSE as SO-RE for sparse datasets such as temperature and salinity profiles. However, OV-RE is a much more flexible scheme, and in fact it has been shown to be capable of assimilating Lagrangian trajectories and gliders (Dobricic et al. 2010)

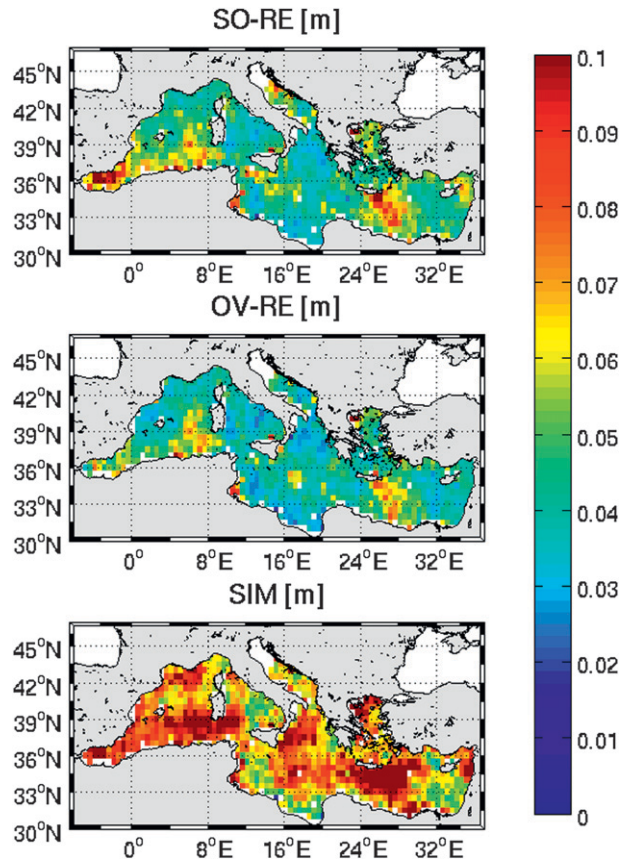


FIG. 18. The 2000–07 time mean RMSE for SLA for (top) OV-RE, (middle) SO-RE, and (bottom) SIM.

easily, which are other important monitoring datasets for the ocean.

It would be desirable in the future to carry out longer reanalyses with the awareness that in the high-resolution regional reanalyses atmospheric forcing uncertainties are probably very important and should be considered in the assimilation scheme.

Acknowledgments. This work was supported by the European Commission MyOcean Project (SPA.2007.1.1.01—development of upgrade capabilities for existing GMES fast-track services and related operational services; Grant Agreement 218812-1-FP7-SPACE 2007-1) and by the CIRCE project, funded by the European Commission's sixth Framework Programme through Contract 036961. We would also like to thank the Istituto Nazionale di Geofisica e Vulcanologia (INGV) and the Centro Euro-Mediterraneo per i Cambiamenti Climatici (CMCC) for facilities support. I am thankful to Dr. P. Oddo and Dr. M. Vichi for the interesting discussions. I am personally grateful to Dr. I. Fukumori for his moral, scientific, and financial support.

APPENDIX A

Model Equations

The model equations are

$$\frac{\partial u}{\partial t} = (\zeta + f)v - w \frac{\partial u}{\partial z} - \frac{1}{2a \cos \phi} \frac{\partial}{\partial \lambda} (u^2 + v^2) - \frac{1}{\rho_o a \cos \phi} \frac{\partial p}{\partial \lambda} - A^{\text{vm}} \nabla^4 u + \frac{\partial}{\partial z} \left(A^{\text{vm}} \frac{\partial u}{\partial z} \right), \quad (\text{A1})$$

$$\frac{\partial v}{\partial t} = -(\zeta + f)u - w \frac{\partial v}{\partial z} - \frac{1}{2a \sin \phi} \frac{\partial}{\partial \phi} (u^2 + v^2) - \frac{1}{\rho_o a} \frac{\partial p}{\partial \phi} - A^{\text{vm}} \nabla^4 v + \frac{\partial}{\partial z} \left(A^{\text{vm}} \frac{\partial v}{\partial z} \right), \quad (\text{A2})$$

$$\frac{\partial p}{\partial z} = -\rho g, \quad (\text{A3})$$

$$\frac{1}{a \cos \phi} \left[\frac{\partial u}{\partial \lambda} + \frac{\partial}{\partial \phi} (\cos \phi v) \right] + \frac{\partial w}{\partial z} = 0, \quad (\text{A4})$$

$$\frac{\partial \theta}{\partial t} = -\frac{1}{a \cos \phi} \left[\frac{\partial}{\partial \lambda} (\theta u) + \frac{\partial}{\partial \phi} (\cos \phi \theta v) \right] - \frac{\partial}{\partial z} (\theta w) - A^{\text{IT}} \nabla^4 T + A^{\text{VT}} \frac{\partial^2 \theta}{\partial z^2} + \delta \mu (\theta^* - \theta), \quad (\text{A5})$$

$$\frac{\partial S}{\partial t} = -\frac{1}{a \cos \phi} \left[\frac{\partial}{\partial \lambda} (S u) + \frac{\partial}{\partial \phi} (\cos \phi S v) \right] - \frac{\partial}{\partial z} (S w) - A^{\text{IS}} \nabla^4 S + A^{\text{VS}} \frac{\partial^2 S}{\partial z^2} + \delta \mu (S^* - S), \quad \text{and} \quad (\text{A6})$$

$$\rho = \rho(T, S, p). \quad (\text{A7})$$

The momentum equation are reformulated as function of the vorticity $\zeta = [1/(a \cos \phi)][\partial v/\partial \lambda + \partial/\partial \phi(u \cos \phi)]$; u , v , w are the components of the velocity vector, a is Earth's radius, $f = 2\Omega \sin \phi$ is the Coriolis term where Ω is the constant Earth rotation rate, p is the hydrostatic pressure, θ is the potential temperature, S is the salinity, ρ is the in situ density, and $\rho_o = 1020 \text{ kg m}^{-3}$ is the reference density. Here, A^{lm} , A^{vm} are the horizontal and vertical eddy viscosities, respectively; A^{VT} , A^{VS} are the vertical diffusivity coefficients; and A^{IT} , A^{IS} are the horizontal diffusivity coefficients for temperature and salinity, respectively; μ and δ are relaxation coefficients. The model also integrates a free surface equation with an implicit scheme. The numerical implementation of the implicit free surface scheme is described in Roulet and Madec (2000).

In our particular implementation, the terms with δ , μ are taken to be zero everywhere except along the borders of the Atlantic box, as described by Tonani et al. (2008a). There is no other interior relaxation in the model

domain. The vertical mixing scheme used in Pacanowski and Philander (1981) and the convective mixing is done by increasing the value of the vertical diffusivity.

To solve the model equations described above it is necessary to impose boundary conditions at the vertical and lateral boundaries.

For the vertical velocity, the boundary condition at the bottom ($z = -\mathbf{H}$) is

$$w = -\mathbf{u}_h^b \cdot \nabla \mathbf{H}, \quad (\text{A8})$$

where \mathbf{u}_h^b is the latitudinal and zonal component of the bottom velocity. At the surface ($z = \eta$), the vertical boundary condition for w is

$$w = \frac{D\eta}{Dt} - \text{WF}, \quad (\text{A9})$$

where WF is the imposed water flux.

The vertical boundary condition for the horizontal velocity components are at the bottom

$$A^{\text{vm}} \frac{\partial \mathbf{u}_h}{\partial z} \Big|_{z=-\mathbf{H}} = C_D \sqrt{u_b^2 + v_b^2} + e_b \mathbf{u}_h^b, \quad (\text{A10})$$

where C_D is the drag coefficient and e_b is the bottom kinetic energy resulting from the tides, internal wave breaking, and other processes characterized by short temporal and spatial scales. The corresponding boundary condition at the surface is

$$A^{\text{vm}} \frac{\partial \mathbf{u}_h}{\partial z} \Big|_{z=\eta} = \frac{\boldsymbol{\tau}}{\rho_o}, \quad (\text{A11})$$

where $\boldsymbol{\tau}$ is the wind stress.

The boundary condition for the temperature and salt flux at the bottom is

$$A^{\text{VT},S} \frac{\partial}{\partial z} (T, S) \Big|_{z=-\mathbf{H}} = 0, \quad (\text{A12})$$

while at the surface

$$A^{\text{VT}} \frac{\partial T}{\partial z} \Big|_{z=0} = \frac{Q_c}{\rho_o C_p}, \quad (\text{A13})$$

and C_p is the specific heat capacity and Q_c is the corrected net heat flux; that is,

$$Q_c = Q_0 + \frac{DQ}{DT} (T_m - T_0). \quad (\text{A14})$$

Here Q_0 is computed by bulk formulas and, in particular,

$$Q_0 = Q_{sw} - Q_{lw} - Q_h - Q_l. \quad (A15)$$

The downward shortwave component (Q_{sw}) is computed using Reed’s (1977) formula, and the upward longwave radiation (Q_{lw}) is computed using Bignami et al.’s (1995) formula. The sensible heat flux is $Q_h = \rho_a C_p C_h |V| (T_s - T_a)$ and the latent heat flux is $Q_l = \rho_a C_e L_e |V| (q_s - q_a)$.

Here, $|V|$ is the wind speed, ρ_a is the density of the moist air, C_p is the specific heat capacity, C_h and C_e are turbulent exchange coefficients for temperature and humidity, L_e is the latent heat of vaporization, q_a is the specific humidity of air, and q_s is the specific humidity saturated at temperature T_s . The second rhs term in Eq. (A14) is the relaxation term, where DQ/DT is equal to $-60 \text{ W m}^{-2} \text{ K}^{-1}$, T_m is the model SST, and T_0 is the OI satellite SST.

For the salinity, the salt flux, corresponding to the water flux is

$$A \text{ vs } \left. \frac{\partial S}{\partial z} \right|_{z=0} = \text{WF } S_{z=0} \rho_o, \quad (A16)$$

and

$$\text{WF}(x, y, t) = E(x, y, t) - P(x, y, tm) - \frac{R(x, y, tm)}{A(x, y)}, \quad (A17)$$

where E is the evaporation, P is the precipitation, R is the runoff, A is the area of each cell of the model that is intersected by the river runoff, (x, y) are the coordinates of the model, t is the model time step, and tm is the monthly time step.

River discharge $R \text{ (m}^3 \text{ s}^{-1}\text{)}$, is multiplied by a Gaussian function at the river mouth. The function is

$$f(r) = \left[1 - \left(\frac{r}{L} \right)^2 \right] \exp \left[-\frac{1}{2} \left(\frac{r}{B} \right)^2 \right], \quad (A18)$$

where r is the distance from the river mouth in the offshore direction. This particular implementation of the model is partially described in Tonani et al. (2008a) and Oddo et al. (2009), and it is also part of the suite of operational models running in the Mediterranean Sea.

APPENDIX B

Numerical Error in the Heat Budget Computation Using Different Time Steps

Here we discuss the estimate of the numerical error term $\varepsilon(\Delta t)$ in Eq. (7). During the model integration, the

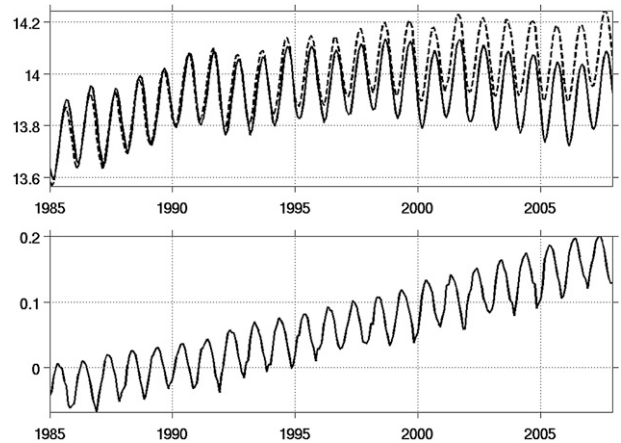


FIG. B1. (top) Basin mean volume temperatures ($^{\circ}\text{C}$) computed using the rhs of Eq. (7) and 1-month time step (dashed line) and the basin mean volume temperature obtained from the average of the model solution every 10-min time step (continuous line). (bottom) Temperature difference ($^{\circ}\text{C}$) between the two estimates.

model time step is $\Delta t = 600 \text{ s}$, while in our diagnostic computation we use a time step of 1 month. Thus, in our diagnostic Eq. (7) we consider a numerical error term resulting from this numerical difference. In the upper panel of Fig. B1, the basin mean temperature computed from the monthly mean average of the model solution each 600 s is shown, together with the evaluation of the same quantity from the rhs of Eq. (7) for SIM. In the lower panel of Fig. B1 we show the difference between these two values, which we argue corresponds to $\varepsilon(\Delta t)$.

REFERENCES

Bignami, F., S. Marullo, R. Santoleri, and M. E. Schiano, 1995: Longwave radiation budget in the Mediterranean Sea. *J. Geophys. Res.*, **100**, 2501–2514.

Bozec, A., P. Bouruet-Aubertot, K. Béranger, and M. Crépon, 2006: Mediterranean oceanic response to the interannual variability of a high-resolution atmospheric forcing: A focus on the Aegean Sea. *J. Geophys. Res.*, **11**, C111013, doi:10.1029/2005JC003427.

Buongiorno Nardelli, B., G. Larnicol, E. D’Acunzo, R. Santoleri, S. Marullo, and P. Y. Le Traon, 2003: Near real time SLA and SST products during 2-years of MFS pilot project: Processing, analysis of the variability and of the coupled patterns. *Ann. Geophys.*, **21**, 103–121.

Carton, J. A., G. Chepurin, and X. Cao, 2000: A simple ocean data assimilation analysis of the global upper ocean 1950–95. Part I: Methodology. *J. Phys. Oceanogr.*, **30**, 294–309.

De Mey, P., and M. Benkiran, 2002: A multivariate reduced-order optimal interpolation method and its application to the Mediterranean Basin-scale circulation. *Ocean Forecasting: Conceptual Basis and Applications*, N. Pinardi and J. Woods, Eds., Springer, 281–306.

- Demirov, E., and N. Pinardi, 2002: Simulation of the Mediterranean Sea circulation from 1979 to 1993. Part I: The interannual variability. *J. Mar. Syst.*, **33–34**, 23–50.
- , and —, 2007: On the relationship between the water mass pathways and eddy variability in the Western Mediterranean Sea. *J. Geophys. Res.*, **112**, C02024, doi:10.1029/2005JC003174.
- Dobricic, S., 2005: New mean dynamic topography of the Mediterranean calculated from assimilation system diagnostics. *Geophys. Res. Lett.*, **32**, L11606, doi:10.1029/2005GL022518.
- , and N. Pinardi, 2008: An oceanographic three-dimensional assimilation scheme. *Ocean Modell.*, **22**, 89–105.
- , —, M. Adani, A. Bonazzi, C. Fratianni, and M. Tonani, 2005: Mediterranean Forecasting System: An improved assimilation scheme for sea-level anomaly and its validation. *Quart. J. Roy. Meteor. Soc.*, **131**, 3627–3642.
- , —, —, M. Tonani, C. Fratianni, A. Bonazzi, and V. Fernandez, 2007: Daily oceanographic analyses by Mediterranean Forecasting System at the basin scale. *Ocean Sci.*, **3**, 149–157.
- , —, P. Testor, and U. Send, 2010: Impact of data assimilation of glider observations in the Ionian Sea (Eastern Mediterranean). *Dyn. Atmos. Oceans*, **50**, 78–92.
- Dougllass, E., D. Roemmich, and D. Stammer, 2009: Data sensitivity of the ECCO state estimate in a regional setting. *J. Atmos. Oceanic Technol.*, **26**, 2420–2443.
- Fu, L.-L., E. Christensen, C. Yamarone, M. Lefebvre, Y. Menard, M. Dorrer, and P. Esudier, 1994: TOPEX/POSEIDON mission overview. *J. Geophys. Res.*, **99**, 24 369–24 381.
- Fukumori, I., 2002: A partitioned Kalman filter and smoother. *Mon. Wea. Rev.*, **130**, 1370–1383.
- Gertman, I., N. Pinardi, Y. Popov, and A. Hecht, 2006: Aegean Sea water masses during the early stages of the Eastern Mediterranean Climatic Transient (1988–1990). *J. Phys. Oceanogr.*, **36**, 1841–1859.
- Gibson, J. K., P. Kallberg, S. Uppala, A. Hernandez, A. Nomura, and E. Serrano, 1997: ERA description. ECMWF Reanalysis Project Rep. Series 1, 86 pp.
- Glickman, T. Ed., 2000: *Glossary of Meteorology*. 2nd ed. Amer. Meteor. Soc., 855 pp.
- Hurrell, J. W., Y. Kushnir, and M. Visbeck, 2001: The North Atlantic Oscillation. *Science*, **291**, 603–605.
- Kistler, R., and Coauthors, 2001: The NCEP–NCAR 50-Year Reanalysis: Monthly means CD-ROM and documentation. *Bull. Amer. Meteor. Soc.*, **82**, 247–268.
- Korres, G., N. Pinardi, and A. Lascaratos, 2000: The ocean response to low-frequency interannual atmospheric variability in the Mediterranean Sea. Part I: Sensitivity experiments and energy analysis. *J. Climate*, **13**, 705–731.
- Madec, G., P. Delecluse, M. Imbard, and C. Levy, 1998: OPA 8.1 ocean general circulation model reference manual. Institut Pierre-Simon Laplace, Note du Pole de Modelisazion, No. 11, 91 pp. [Available online at http://www.nemo-ocean.eu/content/download/259/1665/version/1/file/Doc_OPA8.1.pdf]
- Maillard, C., and Coauthors, 2005: MEDAR/MEDATLAS 1998–2001: A Mediterranean and Black Sea oceanographic data base and network. *Boll. Geofis. Teor. Appl.*, **46**, 329–344.
- Malanotte-Rizzoli, P., B. B. Manca, M. Ribera d’Alcala, A. Theocharis, S. Brenner, G. Budillon, and E. Ozsoy, 1999: The Eastern Mediterranean in the 80s and in the 90s: The big transition in the intermediate and deep circulations. *Dyn. Atmos. Oceans*, **29**, 365–395.
- Manzella, G. M. R., and Coauthors, 2007: The improvements of the ships of opportunity program in MFS-TEP. *Ocean Sci.*, **3**, 245–258.
- Marullo, S., B. Buongiorno Nardelli, M. Guarracino, and R. Santoleri, 2007: Observing the Mediterranean Sea from space: 21 years of Pathfinder-AVHRR sea surface temperatures (1985 to 2005): Re-analysis and validation. *Ocean Sci.*, **3**, 299–310.
- Masina, S., P. Di Pietro, and A. Navarra, 2004: Interannual-to-decadal variability of the North Atlantic from an ocean data assimilation system. *Climate Dyn.*, **23**, 531–546.
- Oddo, P., M. Adani, N. Pinardi, C. Fratianni, M. Tonani, and D. Pettenuzzo, 2009: A nested Atlantic-Mediterranean Sea general circulation model for operational forecasting. *Ocean Sci.*, **5**, 461–473.
- Olita, A., R. Sorgente, S. Natale, S. Gabersek, A. Ribotti, A. Bonanno, and B. Patti, 2007: Effects of the 2003 European heatwave on the Central Mediterranean Sea: Surface fluxes and the dynamical response. *Ocean Sci.*, **3**, 273–289.
- Pacanowski, R. C., and S. G. H. Philander, 1981: Parameterization of vertical mixing in numerical modes of tropical oceans. *J. Phys. Oceanogr.*, **11**, 1443–1451.
- Pettenuzzo, D., W. G. Large, and N. Pinardi, 2010: On the corrections of ERA-40 surface flux products consistent with the Mediterranean heat and water budgets and the connection between basin surface total heat flux and NAO. *J. Geophys. Res.*, **115**, C06022, doi:10.1029/2009JC005631.
- Pinardi, N., and E. Masetti, 2000: Variability of the large-scale general circulation of the Mediterranean Sea from observations and modelling: A review. *Palaeogeogr. Palaeoclimatol. Palaeoecol.*, **158**, 153–173.
- , and J. Woods, 2002: *Ocean Forecasting: Conceptual Basis and Applications*. Springer, 472 pp.
- , and Coauthors, 2003: The Mediterranean ocean forecasting system: First phase of implementation (1998–2001). *Ann. Geophys.*, **21**, 3–20.
- , E. Arneri, A. Crise, M. Ravaioli, and M. Zavatarelli, 2006: The physical, sedimentary and ecological structure and variability of shelf areas in the Mediterranean Sea. *The Sea*, A. R. Robinson and K. Brink, Eds., *The Global Coastal Ocean*, Vol. 14b, Harvard University Press, 1243–1330.
- Poulain, P. M., and Coauthors, 2007: MedArgo: A drifting profiler program in the Mediterranean Sea. *Ocean Sci.*, **3**, 379–395.
- Pujol, M.-I., and G. Larnicol, 2005: Mediterranean Sea eddy kinetic energy variability from 11 years of altimetric data. *J. Mar. Syst.*, **58**, 121–141.
- Reed, R. K., 1977: On estimating insolation over the ocean. *J. Phys. Oceanogr.*, **7**, 482–485.
- Rio, M.-H., P.-M. Poulain, A. Pascual, E. Mauri, G. Larnicol, and R. Santoleri, 2007: A mean dynamic topography of the Mediterranean Sea computed from altimetric data, in situ measurements and a general circulation model. *J. Mar. Syst.*, **64**, 484–508.
- Robinson, A. R., W. G. Lesile, A. Theocharis, and A. Lascaratos, 2001: Mediterranean Sea circulation. *Encyclopedia of Ocean Sciences*, J. H. Steele, S. A. Thorpe, and K. K. Turekian, Eds., Academic Press, 1689–1706.
- Roether, W., B. B. Manca, B. Klein, D. Bregant, D. Georgopoulos, V. Beitzel, V. Kovacevic, and A. Lucchetta, 1995: Recent

- changes in the eastern Mediterranean deep waters. *Science*, **271**, 333–335.
- Roullet, G., and G. Madec, 2000: Salt conservation, free surface, and varying levels: A new formulation for ocean general circulation model. *J. Geophys. Res.*, **105** (C10), 23 927–23 942.
- Stammer, D., and Coauthors, 2002: The global ocean circulation during 1992–1997, estimated from ocean observations and a general circulation model. *J. Geophys. Res.*, **107**, 3118, doi:10.1029/2001JC000888.
- Talagrand, O., 1972: On the damping of high-frequency motions in four-dimensional assimilation of meteorological data. *J. Atmos. Sci.*, **29**, 1571–1574.
- Tonani, M., N. Pinardi, S. Dobricic, M. I. Pujol, and C. Fratianni, 2008a: A high-resolution free-surface model of the Mediterranean Sea. *Ocean Sci.*, **4**, 1–14.
- , and Coauthors, 2008b: The Mediterranean ocean forecasting system, coastal to global operational oceanography: Achievements and challenges. *Proc. Fifth EuroGOOS Conf.*, Exeter, United Kingdom, EuroGOOS, Publ. 28.